Real-time monitoring of ^{13}C and ^{18}O-isotopes of human breath CO_2 using a mid-infrared hollow waveguide gas sensor

Tao Zhou, Tao Wu, * Qiang Wu, * Weidong Chen, Mingwei Wu, Chenwen Ye, Xingdao He

ABSTRACT: Real-time measuring CO_2 isotopes ($^{13}CO_2$, $^{12}CO_2$, and $^{18}OC^{16}O$) in exhaled breath using a mid-infrared hollow waveguide (HWG) gas sensor incorporating a 2.73 μm DFB laser was proposed and demonstrated first time based on calibration-free wavelength modulation spectroscopy (CF-WMS). The measurement precisions for $\delta^{13}C$ and $\delta^{18}O$ were respectively 0.26‰ and 0.57‰ for an integration time of 131 s by Allan variance analysis. These measurement precisions achieved in the present work were at least 3.5 times better than those reported using direct absorption spectroscopy (DAS) and 1.3 times better than those obtained by calibration-needed wavelength modulation absorption spectroscopy (CN-WMS). Continuous measurement of three isotopes in the breathing cycle was performed. Alveolar gas from the expirogram was identified, and the $^{13}C/^{12}C$ and $^{18}O/^{16}O$ ratios were found to be almost constant during the alveolar plateau, which enables optimization of breath sampling and providing accurate information on metabolic processes. The $^{13}C/^{12}C$ and $^{18}O/^{16}O$ isotope ratios at the alveolar plateau of five breath cycles were averaged, yielding $\delta^{13}C$ and $\delta^{18}O$ values of (-24.3±3.4) ‰ and (-30.7±2.6) ‰, respectively. This study demonstrates the feasibility of real-time analysis of ^{13}C and ^{18}O-isotopes of human breath CO_2 in clinical application and shows its potential for diagnosing respiratory-related diseases with high sensitivity, selectivity, and specificity.

Helicobacter pylori (H. pylori) is a well-known pathogen that causes chronic gastritis, peptic ulcers, gastric cancer, and mucosa-associated lymphoid tissue lymphoma [1-2]. Though harmful acidic environment in the gastrointestinal tract, it can generate large quantities of urease to hydrolyze urea, thereby releasing ammonia (NH_3) and carbon dioxide (CO_2) gas and offering a protective alkaline environment. Therefore, H. pylori would be diagnosed with recognizing its urease enzyme activity. By taking a small amount of ^{13}C-labeled pills, a suspected H. pylori patient will exhibit enrichment of $^{13}CO_2$ in the exhaled gas, which is usually reported as the delta over baseline (DOB) value relative to a standard [3-4]. Recently, the ^{18}O-isotope of CO_2 in exhaled gas was also demonstrated as a potential molecular biomarker to track the pathogenesis of H. pylori [5] distinctively. A $\delta_{DOB}{}^{13}C \geq 2.0‰$ or $\delta_{DOB}{}^{18}O \geq 1.92‰$ is strongly relevant with the infection of H. pylori in the human stomach [6-7]. ^{18}O and ^{13}C isotopes were also reported for possibly tracking the coexistence of H. Pylori infection and type 2 diabetes (T2D) [8]. Thus they also might be considered as potential biomarkers for the non-invasive assessment of the gastric pathogen prior to the onset of T2D [8]. For traditional offline breath analysis, exhaled gases are collected in sampling bags, and changes of isotopes δ values of exhaled gases before and after ^{13}C-enriched pills ingestion are used to judge diseases. However, this method may be affected by the contamination of alveolar gas with the dead space gas [9] and result in misdiagnosis. Meanwhile, the quantitative determination of a specific metabolic process is missing. Direct online real-time analyses of every single breath enable identifying alveolar gas from the expirogram, quantitative determination of metabolization dynamics, accounting for the variability stemming from varying physiological states, and extracting physiological parameters [10-11]. Therefore, real-time, in-situ, and accurate determination of $\delta^{13}C$ and $\delta^{18}O$ is essential in the breath diagnostic analysis.

Various technologies were developed to measure stable isotopologues of CO_2 for studies of the global carbon cycle and climate change, such as isotope ratio mass spectrometry (IRMS) [12], Fourier transform infrared (FTIR) spectroscopy [13] and laser absorption spectroscopy [14-17]. Although IRMS has high measurement accuracy and sensitivity, it also has some limits such as complicated operation, high cost, bulky equipment, and time-consuming pretreatment of samples. FTIR is also a well-established method. However, it requires high-cost instruments and long measurement time. Laser absorption spectroscopy possesses unique advantages, such as fast response, small size, high spectral resolution, simple operation, high detection sensitivity, and real-time online analysis. Therefore, laser absorption spectroscopy like photoacoustic spectroscopy (PAS), cavity-enhanced absorption spectroscopy (CEAS), cavity ring-down spectroscopy (CRDS), and tunable diode laser absorption spectroscopy (TDLAS) are widely used in the real-time measurement of CO_2 isotopes for not only at the atmosphere but also in breath gas [14-17]. However, actual real-time measurement needs a sampling system with low volume for fast gas exchange. Compared with traditional sampling cell such as multi-pass cell and high finesse optical cavity, hollow waveguide (HWG) has a small volume (~1 ml), resulting in a rapid renewal of respiratory gas in the cell and a fast response time (~3 s). Hence, it is an ideal sampling cell for breath analysis [18-20]. Moreover, till now, only a few literatures reported measurement of $\delta^{18}O$ in exhaled CO_2 gas [7-8, 21-22].

In our previous work, we measured the concentration changes of the three isotopologues $^{13}CO_2$, $^{12}CO_2$, and $^{18}OC^{16}O$ in exhaled breath by DAS technique [23]. The WMS enable effectively suppress the $1/f$ noise by using a higher modulation frequency (~kHz) and hence sensitivity using WMS is usually higher than that using DAS. In traditional CN-WMS technique, signals are calibrated by using standard gases with known concentrations, which is complicate and costly. For CF-WMS

technique, the gas concentrations are retrieved by fitting the simulated 2f signals to measured signals without calibration process, and thus the measurement results are more accurate. In this paper, we demonstrated real-time detection of CO_2 and its isotopes in breathing gas using a 1 m long HWG by the CF-WMS technique. A 2.73 μm DFB laser was selected as light source to target absorption lines of CO_2 isotopes. CF-WMS and CN-WMS techniques were used to retrieve concentrations of CO_2 isotopes and then to determine $\delta^{13}C$ and $\delta^{18}O$ with high precision. The results obtained by CF-WMS, CN-WMS, and DAS techniques are compared. We measured sequences of three CO_2 isotopes expirograms during tidal-breathing in a healthy volunteer by the CF-WMS technique. Real-time monitoring $^{13}C/^{12}C$ and $^{18}O/^{16}O$ isotope ratios during tidal-breathing were achieved, and $\delta^{13}C$ and $\delta^{18}O$ values in exhaled gases were determined.

In the WMS technique, after superimposition of high-frequency sine wave signal on the injection current of the DFB laser, the frequency of the laser is modulated and given by

$$\nu(t) = \nu_c + \nu_a \cos(2\pi ft) \tag{1}$$

where ν_c is the center frequency of a laser, ν_a and f are the modulation amplitude and frequency, respectively.

After the laser passes the sample with absorbance $\alpha(\nu)<0.05$, the detector signal $S[\nu(t)]$ is expressed by

$$S[\nu(t)] \approx \eta I_0\{1-\alpha[\nu_d + \nu_a \cos(2\pi ft)]\} \tag{2}$$

where η is the photoelectric conversion coefficient of the photodetector. I_0 are the intensity of incident light. ν_d is the detuning frequency. The absorbance can conveniently be expressed as an area-normalized linear function $\chi(\nu)$ alternatively as

$$\alpha(\nu) = S\chi(\nu)n_aL = S\chi(\nu)Cn_{tot}L \tag{3}$$

where S and C are the line strength and concentration of the absorber, respectively. L is the interaction length. n_a and n_{tot} are the density and total number density of absorbers, respectively.

The in and out of phase components of the nth harmonic from the lock-in amplifier, $S_n^{in}(\nu_d,\nu_a)$ and $S_n^{out}(\nu_d,\nu_a)$, are in proportion to the even and odd components of the nth Fourier coefficient of the detector signal, $S_n^{even}(\nu_d,\nu_a)$ and $S_n^{odd}(\nu_d,\nu_a)$, which can be expressed as [24]:

$$S_n^{in}(\nu_d,\nu_a) = \beta S_n^{even}(\nu_d,\nu_a) \tag{4}$$

$$S_n^{out}(\nu_d,\nu_a) = \beta S_n^{odd}(\nu_d,\nu_a) \tag{5}$$

where β is the gain of the lock-in amplifier.

If the modulated signal is pure cosine modulation and there is no phase delay between absorption and modulation frequency, all odd components is zero. The nth harmonic signal from the lock-in amplifier can be written as [24]:

$$S_n^{in}(\nu_d,\nu_a) = -\beta\eta I_0 Sn_aL\chi_n^{even}(\nu_d,\nu_a) \tag{6}$$

where $\chi_n^{even}(\nu_d,\nu_a)$ is the even components of the nth Fourier coefficient of the modulated line-shape function. When pressure broadening dominates, the line shape becomes Lorentzian. For 2f signals' detection, lock-in output originating from a Lorentzian line-shape is given by [24]:

$$S_{2,L}^{in}(\bar{\nu}_d,\bar{\nu}_a) = -\beta\eta I_0 Sn_aL\chi_{2,L}^{even}(\bar{\nu}_d,\bar{\nu}_a) \tag{7}$$

where $\bar{\nu}_d(\nu_d/\Delta\nu_L)$ and $\bar{\nu}_a(\nu_a/\Delta\nu_L)$ are width-normalized frequency and modulation amplitude, respectively, $\Delta\nu_L$ is the half width at half maximum (HWHM) of the Lorentzian profile, and $\chi_{2,L}^{even}(\bar{\nu}_d,\bar{\nu}_a)$ is the second harmonic of the wavelength modulated area-normalized Lorentzian shaped lineshape function [25].

The parameters β, η, I_0, S and L in Eq. (7) are fixed, and the value of $\beta\eta I_0 SL$ can be determined by measuring the gas with known concentration. According to Eq. (7), the 2f signal is the function of the density of absorbers n_a and the line-shape function $\chi_{2,L}^{even}(\bar{\nu}_d,\bar{\nu}_a)$, which depends on the transition center frequency ν_o and the lineshape parameter $\Delta\nu_L$. The simulated 2f signal is used to match the measured spectra by a least-square method, where the value of density of absorbers n_a and then the gas concentration C can be determined based on the best fit.

The change in isotope abundance is generally expressed by R, which is the concentration ratio of heavy to light isotopes:

$$R = C^x / C^a \tag{8}$$

where x and a refer to heavy isotopic species ($^{13}CO_2$, $^{18}OC^{16}O$) and light isotopic component ($^{12}CO_2$), respectively. Stable isotope ratio is usually expressed in per mil (‰) relative to the Vienna Pee Dee Belemnite (VPDB) standard, the so-called δ-value. Unknown $\delta^{13}C$ and $\delta^{18}O$ of the gas samples are calculated using $\delta^{13}C_{cal}$ and $\delta^{18}O_{cal}$ of the calibration gas, respectively [26]:

$$\delta^{13}C = \delta^{13}C_{cal} + \frac{R_{sam}-R_{cal}}{R_{VPDB}^{13}} \tag{9}$$

$$\delta^{18}O = \delta^{18}O_{cal} + \frac{R_{sam}-R_{cal}}{R_{VPDB-CO2}^{18}} \tag{10}$$

where R_{sam} and R_{cal} are measured ratios of heavy/light isotopes for gas samples and calibration gas, respectively. R_{VPDB}^{13} =0.0111802 is the standard molar ratio of $^{13}C/^{12}C$ for the VPDB scale. $R_{VPDB-CO2}^{18}$ =0.00208835 is the standard molar ratio of $^{18}O/^{16}O$ for the VPDB-CO_2 scale.

The main absorption bands for measuring CO_2 isotopes by laser spectroscopy are the ν3 band located at 4.3 μm, the ν2 band centered at 1.5 μm and the ν1+ν3 band centered at 2.7 μm. Since line intensities at 1.5 μm are one hundred times weaker than that of ν1 +ν3 band, the absorption cell with an effective optical path of several kilometers is used indispensably. Though absorption of CO_2 at 4.3 μm are hundreds of times stronger than that of the ν1+ν3 band, commercially available compact and cheap DFB lasers at 2.73 μm combined with WMS method are also key factors to the choice of CO_2 isotopes measurement method. For the selection of the most appropriate isotopes absorption lines, several important points must be considered. Firstly, the lines should be free of interference with other isotopes or other molecules. Secondly, each isotope should be of similar intensities and similar ground state energy. Finally, all isotopes should lie within the laser wavelength tuning range.

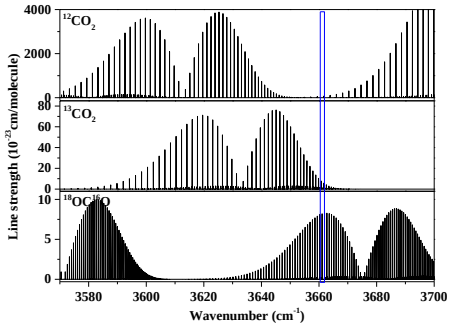

Figure 1 Absorption lines of CO_2 for three different isotopes: $^{12}CO_2$, $^{13}CO_2$, and $^{18}OC^{16}O$ at 2.73 μm.

Figure 1 shows the simulation of this spectral region according to the HITRAN 2016 database [27].The most suitable line pair that satisfies these conditions around 2.73 μm is centered at 3661.4948 cm^{-1} ($^{12}CO_2$), 3661.0834 cm^{-1} ($^{18}OC^{16}O$) and 3660.7693 cm^{-1} ($^{13}CO_2$), the corresponding absorption line strength were 7.79×10^{-23} cm/molecule, 8.19×10^{-23} cm/molecule and 4.917×10^{-23} cm/molecule respectively [23].

The temperature sensitivity of the isotopic ratio is proportional to the difference of the ground-state energies. The sensitivities of the isotope ratios for selected line pair is given as -9.6‰/K and -26.7‰/K for the $\delta^{13}C$ and $\delta^{18}O$, respectively [23].

EXPERIMENTAL SECTION

A schematic diagram of the proposed mid-infrared HWG CO_2 isotopes sensor system for breathing gas is shown in Figure 2(a). The sensor system was mainly divided into three parts: optical platform, signal controlling and acquisition system, and gas handling system. On the optical platform, the laser employed was a tunable DFB laser operated at wavelength of 2.73 μm by Nanoplus Company with a maximum power of 11.2 mW. It was packaged in a TO-5 package with integrated Peltier and temperature sensors. The light emitted by the laser was collimated by an antireflection coated aspheric lens with a 4 mm focal length (Lightpath, USA) equipped in the laser mount and then focused into a 1 m long HWG (HWEA 10001600, Polymicro Technologies, USA) by a focusing lens. The HWG connector is shown in Figure 2(b). To prevent leakage of the gas from the connector: 1) the HWG fiber is inserted into the slot of the connector and sealed by silicon glue; 2) Calcium Fluoride (CaF2) wedged window is sealed on the connector via an O-ring. The emitting light from the HWG was collected by a photovoltaic detector (PVI-4TE-10.6, VIGO system S.A., USA). To minimize interference from ambient CO_2 and its isotopes, the laser and detector should be close to the HWG. For the signal controlling and acquisition system, a laser controller (LDC-3724, ILX Lightwave, USA) controlled the temperature and current of the laser with a temperature control accuracy of 0.1 ℃ and a current output accuracy of 0.05%. A 20 Hz sawtooth wave generated by a function generator was summed by an adder with a 1.6 kHz high-frequency sine wave generated by a digital lock-in amplifier (SR830, Stanford Research System, USA) and then drive the laser wavelength to perform WMS. The demodulated signal from the digital lock-in amplifier was acquired by a 14-bit analog-to-digital data acquisition card (DAQ-2010, ADlink, China), and then recorded and analyzed by a self-developed Labwindows program.

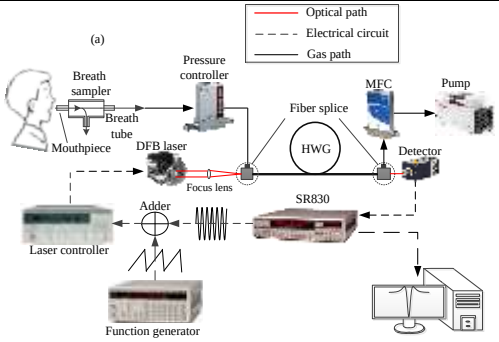

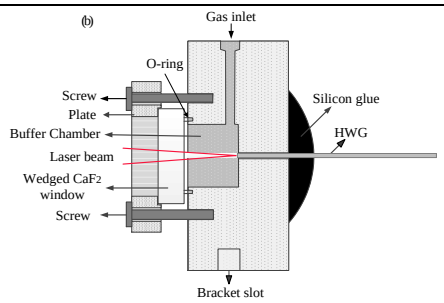

Figure 2 (a) Schematic of the experimental setup for measuring CO_2 isotopes in breathing gas based on HWG, (b) Schematic layout of the hollow waveguide connector.

In the gas handling system, the central part of breathing gas was released to the air by the bypass of breath sampler, only a small part of breathing gas was inhaled to the HWG cell through a diaphragm pump (1.2 L, DIVAC, Germany). One pressure controller (640B, MKS Instruments, USA) at HWG inlet and one mass flow controller (MFC, GV50A, MKS Instruments, USA) at HWG outlet controlled the pressure and flow rate of gas in the HWG, respectively. For preparing dilute standard CO_2 samples, another two MFCs replacing breath sampler were connected to high-purity CO_2 and nitrogen, respectively. A variety of CO_2 concentrations were produced by adjusting the flow rates of two MFCs. The HWG temperature was stabilized at 25 ℃ using a heating plate controlled with a PID temperature controller and a platinum resistor (Pt100).

Figure 3 shows experimental WMS-2f raw signal (black line) of three CO_2 isotopes with 0.54 s integration time (5 averages). The CO_2 sample concentration was 5% at 200 Torr. A least-square fit of a simulated Lorentzian line shape (red line) to the raw signal (black line) and the corresponding fit residual (gray line) were also shown in Figure 3. The relative large residuals around left absorption peaks were caused by spectral fitting algorithm that cannot take into account second harmonic distortions perfectly due to the nonlinearities in the modulation. The concentrations of $^{12}CO_2$, $^{13}CO_2$, $^{18}OC^{16}O$ obtained from the fit were 4.85%, 0.0533%, 0.0194% respectively.

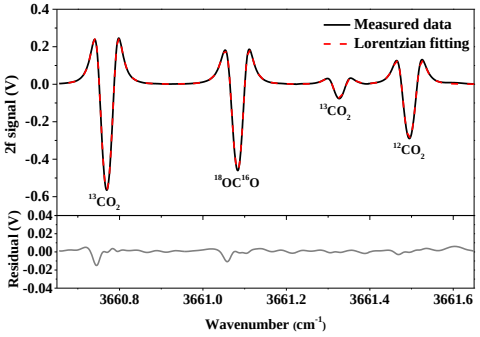

Figure 3 Measured WMS-2f signals of three CO_2 isotopes with least-square Lorentzian fit and fit residual.

The WMS-2f signals of dilute standard CO_2 samples with concentrations of 3%, 4%, 5%, 6%, 7%, and 8% were measured by CF-WMS technique. The concentrations of three CO_2 isotopes were determined by the least-square-fit and plotted in Figure 4. There was a good linear relationship between three CO_2 isotopes concentrations obtained by the CF-WMS technique and standard samples concentrations, with linear correlation coefficients R^2>0.9994. The maximum absolute errors between the measured results and standard sample concentrations were 0.07%, 20.0 ppm, 3.39 ppm for $^{12}CO_2$, $^{13}CO_2$,

$^{18}OC^{16}O$, respectively, and the average absolute errors were 0.045%, 10.2 ppm, 1.46 ppm respectively. These outcomes validate the CF-WMS method, which gives a linear response versus standard gas concentration.

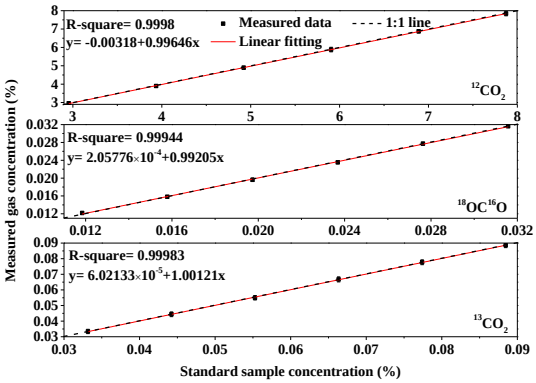

Figure 4 Measured concentrations vs. standard gas concentrations for three CO_2 isotopes.

RESULTS AND DISCUSSION

Evaluation of Response Time. Seven different standard CO_2 samples with concentrations of 0%, 3%, 4%, 5%, 6% and 7%, were applied to investigate the response time of the sensor. According to the natural abundance of $^{12}CO_2$, $^{13}CO_2$ and $^{18}OC^{16}O$, the standard gas concentrations for three CO_2 isotopes are listed in Table 1. Dynamic measurements for different $^{13}CO_2$ levels were shown in Figure 5. The 10–90% response time τ_r and the 0–10% delay time τ_d were investigated. It can be seen from Figure 5 that τ_d in the rising process and the falling process were both 0.54s, while τ_r was 2.7s and 3s, respectively. The response time of the sensor depended on the physical size of the cell, the gas mixing time, the flow rate of gas in the cell, and the processing time of data acquisition and analysis. Due to the fact that no gas mixing required for breath measurement, its response time is shorter than that for measurement of standard CO_2 samples.

Table 1 the standard gas concentrations for three CO_2 isotopes

Total mixing ratio	$^{12}CO_2$	$^{13}CO_2$	$^{18}OC^{16}O$
3%	2.95%	0.0332%	0.0118%
4%	3.93%	0.0442%	0.0158%
5%	4.92%	0.0553%	0.0197%
6%	5.91%	0.0663%	0.0237%
7%	6.89%	0.0774%	0.0276%
8%	7.87%	0.0885%	0.0316%

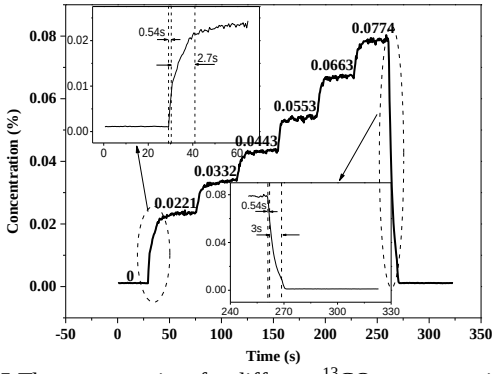

Figure 5 The response time for different $^{13}CO_2$ concentration levels.

Allan Variance Analysis. Allan variance is a widely used method for a comprehensive evaluation of detection limits and system stability [28]. The WMS-2f signals of three CO_2 isotopes for 5% standard CO_2 samples were recorded every 0.54 s for 17 minutes. The concentrations of three CO_2 isotopes were obtained by the CF-WMS technique and peak value calibrated CN-WMS technique, respectively. Then $\delta^{13}C$ and $\delta^{18}O$ (gray lines in Figure 6) were calculated by Equation (8-10) using the calibration gas with $\delta^{13}C$ of -21.34 ‰ and $\delta^{18}O$ of -30.89 ‰, which was determined by an isotope ratio mass spectrometer (IRMS). The precision of $\delta^{13}C$ and $\delta^{18}O$ and the optimum integration time for two techniques were determined by Allan variance analysis. Figure 6 (e) shows the precision of $\delta^{13}C$ and $\delta^{18}O$ were 0.26‰ and 0.57‰ for CF-WMS, while 0.32‰ and 0.74‰ for CN-WMS, respectively, at the optimal integration time of 131s.

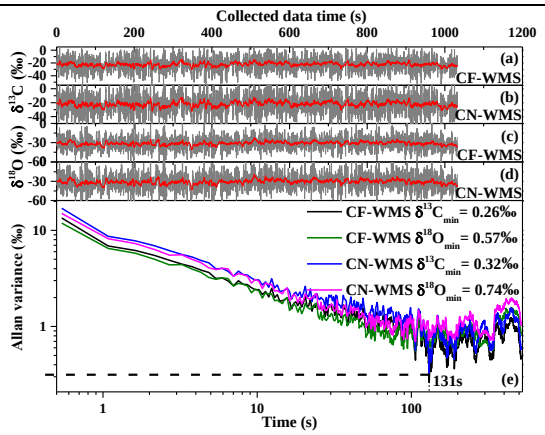

Figure 6 The upper four panels show measured $\delta^{13}C$ and $\delta^{18}O$ (gray lines) and the corresponding FFT filtering results (red lines) by CF-WMS and CN-WMS. The Allan variances plot shows precision of $\delta^{13}C$ and $\delta^{18}O$ and optimal integration time in the lower panel.

In our previous work, we measured the concentrations of the three isotopologues $^{13}CO_2$, $^{12}CO_2$, and $^{18}OC^{16}O$ by DAS technique, where precisions of $\delta^{13}C$ and $\delta^{18}O$ were 2.20‰ and 1.98‰, respectively, at an optimal integration time of 734 s by Allan variance analysis [23]. Table 1 summarizes the comparison of measurement precision obtained by CF-WMS, CN-WMS, and DAS technique. It can be seen from Table 2 that, the precision of the CF-WMS technique was improved at least 3.5 times compared to those reported values using DAS and 1.3 times than those obtained by CN-WMS.

Table 2 The comparison of measurement precision obtained by CF-WMS, CN-WMS and DAS techniques.

Precision	CF-WMS /131 s average	CN-WMS /131 s average	DAS / 734 s average
$\delta^{13}C$ (‰)	0.26	0.32	2.20
$\delta^{18}O$ (‰)	0.57	0.74	1.98

To achieve high time resolution for performing a real-time measurement, 4-point fast Fourier transform (FFT) was employed to smooth successive concentrations of three CO_2 isotopes (red lines in Figure 6). After using 4-point fast FFT smoothing filter, the precision of $\delta^{13}C$ and $\delta^{18}O$ were 2.60‰ and 2.51‰ for CF-WMS, respectively, while 3.28‰ and 3.17‰ for CN-WMS with a 0.54s time resolution. Compared with the multi-point averaging method, the 4-point fast FFT filtering reduces the time of determining δ values (reduced from 131 s to 0.54 s), and thus significantly reduces the response time of the system, with a cost of sacrificing performance of precision.

Real-time Measurement of the Breathing Cycle. Sequences of three CO_2 isotopes expirograms during tidal-breathing at a regular rate in a healthy volunteer were shown in Figure 7. The pressure and gas flow rate in the HWG cell were 200 torr and 3.33 mL/s, respectively. Five consecutive profiles for changes in three CO_2 isotopes concentrations (black line) were determined in real-time by the CF-WMS technique. Then the data was processed by a 4-point fast FFT smoothing filter (red line) and used to calculate $^{13}C/^{12}C$ and $^{18}O/^{16}O$ ratios by Equation (8).

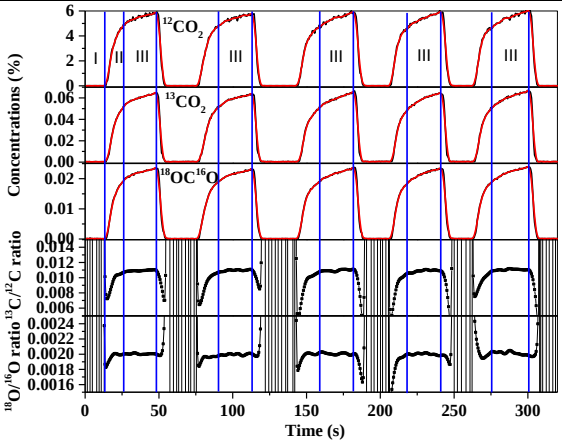

Figure 7 Sequences of three CO_2 isotopes expirograms. CO_2 isotopes concentrations were determined by the CF-WMS technique (black line), and then the data was processed by FFT smoothing filter (red line). Real-time determination of the $^{13}C/^{12}C$ and $^{18}O/^{16}O$ ratios during tidal-breathing was given. Phase I represents the initial status of expiration, phase II shows a sharp rising of the alveolar air, phase III represents the alveolar plateau.

Figure 7 also shows the three different exhalation phases for expirograms of three CO_2 isotopes. Phase I represents the inhaled air in the airways (dead space) in the initial status of expiration. Phase II of the expirogram represents the increasing fraction of the alveolar air resulting in concentrations with the rapidly rising. Phase III describes the air from the alveoli (alveolar plateau) and indicates the alveolar slope. The $^{13}C/^{12}C$ and $^{18}O/^{16}O$ isotope ratios were found to be varied during phase I and II, almost constant during phase III, as shown in Figure 7. The $^{13}C/^{12}C$ and $^{18}O/^{16}O$ isotope ratios for the alveolar plateau of five breath cycles were averaged, which yielded $\delta^{13}C$ and $\delta^{18}O$ values of (-24.3±3.4) ‰ and (-30.7±2.6) ‰, respectively, which reduce measurement errors in breath gas by sampling only alveolar gas and eliminating dead space gas. These determined δ values are compatible with measurement precisions (2.60 ‰ for $\delta^{13}C$ and 2.51 ‰ for $\delta^{18}O$) by using 4-point fast FFT smoothing filter.

CONCLUSIONS

A mid-infrared HWG (1 m long) based sensor prototype for monitoring the $\delta^{13}C$ and $\delta^{18}O$ in breathing gas was demonstrated using the CF-WMS technique. Compared with traditional large size gas cell, this sensor has the advantages of small volume, fast response time, and lightweight, which can be easily used for real-time clinical diagnosis and monitoring of breathing gas. The maximum absolute errors between the measured result and dilute standard sample concentrations were 0.036%, 3.98 ppm, 3.39 ppm for $^{12}CO_2$, $^{13}CO_2$, $^{18}OC^{16}O$, respectively, and average absolute errors were 0.021%, 0.38 ppm, 1.46 ppm. With the optimal integration time of 131 s, the measured precision of $\delta^{13}C$ and $\delta^{18}O$ were 0.26‰ and 0.57‰. The measurement precisions were improved at least 3.5 times compared to those obtained using DAS and 1.3 times than those achieved by CN-WMS. An FFT filter was employed here to smooth concentrations profiles of three CO_2 isotopes and real-time determination of the $^{13}C/^{12}C$ and $^{18}O/^{16}O$ isotope ratios. Sequences of three CO_2 isotopes expirograms were measured by the CF-WMS technique combined with FFT smooth filtering. Real-time monitoring of the $^{13}C/^{12}C$ and $^{18}O/^{16}O$ ratios were achieved during tidal-breathing and it was found to be a constant during the alveolar plateau. The $\delta^{13}C$ and $\delta^{18}O$ values of (-24.3±3.4)‰ and (-30.7±2.6)‰ were obtained based on averaging the $^{13}C/^{12}C$ and $^{18}O/^{16}O$ isotope ratios at the alveolar plateau of five breath cycles, respectively, which reduce measurement errors in breath gas by sampling only alveolar gas and eliminating dead space gas. This work demonstrates that the developed mid-infrared HWG based gas sensor is potential for clinical respiratory monitoring and disease diagnosis.

AUTHOR INFORMATION

Corresponding Author

Tao Wu - *Key Laboratory of Nondestructive Test (Ministry of Education), Nanchang Hangkong University, Nanchang, 330063, China*; E-mail: wutccnu@nchu.edu.cn

Qiang Wu - *Department of Mathematics, Physics and Electrical Engineering, Northumbria University, Newcastle upon Tyne, NE1 8ST, UK*; E-mail: qiang.wu@northumbria.ac.uk

Authors

Tao Zhou, Chenwen Ye, Xingdao He - *Key Laboratory of Nondestructive Test (Ministry of Education), Nanchang Hangkong University, Nanchang, 330063, China*

Weidong Chen - *Laboratoire de Physicochimie de l'Atmosphère, Université du Littoral Côte d'Opale 189A, Av. Maurice Schumann, Dunkerque 59140, France*

Mingwei Wu - *Shenzhen Hospital, Southern Medical University,1333 Xinhu Rd, Shenzhen 518000, China*

Notes

The authors declare no competing financial interest.

ACKNOWLEDGMENT

The authors acknowledge the support of the Key Research and Development Program of Jiangxi Province, China (20192BBH80019) and Natural Science Foundation of Jiangxi Province (Grant No. 20192ACB20031).

REFERENCES

(1) Covacci, A.; Telford, J. L.; Del Giudice, G.; Parsonnet, J.; Rapuoli, R. Helicobacter pylori virulence and genetic geography. *Science* **1999**, *284*, 1328-1333.

(2) El-Omar, E. M.; Carrington, M.; Chow, W. H.; McColl, K. E.; Bream, J. H.; Young, H. A.; Herrera, J.; Lissowska, J.; Yuan, C. C.; Rothman, N.; Lanyon, G.; Martin, M.; Fraumeni, J. F.Jr; Rabkin, C. S. Interleukin-1 polymorphisms associated with increased risk of gastric cancer. *Nature* **2000**, *404*, 398-402.

(3)Savarino, V.; V*igneri*, S.; Celle, G. The 13C urea breath test in the diagnosis of Helic obacter pylori infection. *Gut*. **1999**, *45*, I18-22.

(4) Coelho, L. G. V.; Reber, M.; Passos, M. C. F.; Aguiar, R. O. A.; Casaes, P. E.; Bueno, M. L.; Yazaki F. R.; Castro F. J.; Vieira W. L. S.; Franco J. M. M.; Castro, L. P. Application of isotope-selective non-dispersive infrared spectrometry for the evaluation

of the 13C-urea breath test: comparison with three concordant methods. *Braz. J. Med. Biol. Res*. **1999**, *32*, 1493-1497.
(5) Som, S.; De, A.; Banik, G. D.; Maity, A.; Ghosh, C.; Pal, M.; Daschakraborty, S. B.; Chaudhuri, S.; Jana S; Pradhan, M. Mechanisms linking metabolism of Helicobacter pylori to 18O and 13C-isotopes of human breath CO2. *Sci. Rep*. **2015**, *5*, 10936.
(6) Koletzko, S.; Koletzko, B.; Haisch, M.; Hering, P.; Seeboth, I.; Hengels, K.; Braden, B.; Hering P. Isotope-selective non-dispersive infrared spectrometry for detection of Helicobacter pylori infection with 13C-urea breath test. *Lancet*, **1995**, *345*, 961-962.
(7) Maity, A.; Som, S.; Ghosh, C.; Banik, G. D.; Daschakraborty S. B.; Ghosh, S.; Chaudhuri S.; Pradhan, M. Oxygen-18 stable isotope of exhaled breath CO2 as a non-invasive marker of Helicobacter pylori infection. *J. Anal. At. Spectrom.* **2014**, *29*, 2251-2255.
(8) Som, S., Dutta Banik, G.; Maity, A.; Ghosh, C.; Chaudhuri, S.; Pradhan, M. Non-invasive diagnosis of type 2 diabetes in Helicobacter pylori infected patients using isotope-specific infrared absorption measurements. *Iso. Environ. Healt. S*. **2018**, *54*, 435-445.
(9) Ichinose, Y.; Kanai, E.; Yamasawa, F.; Nishi, I.; Toyama, K. Simultaneous continuous 13C, 12C analysis of expired gas in the 13C breath test. *Respirology* **1998**, *3*, 21-24.
(10)Rubin, T.; Von Haimberger, T.; Helmke, A.; Heyne, K. Quantitative determination of metabolization dynamics by a real-time 13CO2 breath test. *J. Breath Res.* **2011**, *5*, 027102.
(11)King, J.; Unterkofler, K.; Teschl, G.; Teschl, S.; Koc, H.; Hinterhuber, H.; Amann, A. A mathematical model for breath gas analysis of volatile organic compounds with special emphasis on acetone. *J. Math. Biol*. **2011**, *63*, 959-999.
(12)Werner, R. A.; Rothe, M.; Brand, W. A. Extraction of CO2 from air samples for isotopic analysis and limits to ultra high precision δ18O determination in CO2 gas. *Rapid Commun. Mass Sp.* **2001**, *15*, 2152-2167.
(13)Esler, M. B.; Griffith, D. W. T.; Wilson, S. R.; Steele, L. P. Precision trace gas analysis by FT-IR spectroscopy. 2. The 13C/12C isotope ratio of CO2. *Anal. Chem*. **2000**, *72*, 216-221.
(14)Wang, Z.; Wang, Q.; Ching, J. Y. L.; Wu, J. C. Y.; Zhang, G.; Ren, W. A portable low-power QEPAS-based CO2 isotope sensor using a fiber-coupled interband cascade laser. *Sensor Actuat. B: Chem*. **2017**, *246*, 710-715.
(15)Kasyutich, V. L.; Martin, P. A.; & Holdsworth, R. J. An off-axis cavity-enhanced absorption spectrometer at 1605 nm for the 12CO2/13CO2 measurement. *Appl. Phys. B* **2006**, *85*, 413-420.
(16) Crosson, E. R.; Ricci, K. N.; Richman, B. A.; Chilese, F. C.; Owano, T. G.; Provencal, R. A.; Todd, M. W.; Glasser J.; Kachanov, A. A.; Paldus, B. A.; Spence, T. G; Zare, R. N. Stable isotope ratios using cavity ring-down spectroscopy: determination of 13C/12C for carbon dioxide in human breath. *Anal. Chem.* **2002**, *74*, 2003-2007.
(17)Kasyutich, V. L., Martin, P. A. 13CO2/12CO2 isotopic ratio measurements with a continuous-wave quantum cascade laser in exhaled breath. *Infrared Phys. Techn*. **2012**, *55*, 60-66.
(18)Liu, L.; Xiong, B.; Yan, Y.; Li, J.; Du, Z. Hollow waveguide-enhanced mid-infrared sensor for real-time exhaled methane detection. *IEEE Photonic. Techn. L.* **2016**, *28*, 1613-1616.
(19)Wörle, K.; Seichter, F.; Wilk, A.; Armacost, C.; Day, T.; Godejohann, M.; Wachter U.; Vogt, J.; Radermacher, P.; Mizaikoff, B. Breath analysis with broadly tunable quantum cascade lasers. *Anal. Chem*. **2013**, *85*, 2697-2702.
(20)Robinson, I.; Butcher, H. L.; Macleod, N. A.; Weidmann, D. Hollow waveguide integrated laser spectrometer for 13CO2/12CO2 analysis. *Opt. Express* **2019**, *27*, 35670-35688.
(21)Ghosh, C.; Banik, G. D.; Maity, A.; Som, S.; Chakraborty, A.; Selvan, C.; Ghosh, S.; Chowdhury, S.; Pradhan, M. Oxygen-18 isotope of breath CO2 linking to erythrocytes carbonic anhydrase activity: a biomarker for pre-diabetes and type 2 diabetes. *Sci. Rep.* **2015**, *5*, 8137.
(22)Ghosh, C.; Mandal, S.; Banik, G. D.; Maity, A.; Mukhopadhyay, P.; Ghosh, S.; Pradhan, M. Targeting erythrocyte carbonic anhydrase and 18O-isotope of breath CO2 for sorting out type 1 and type 2 diabetes. *Sci. Rep.* **2016**, *6*, 35836.
(23)Zhou, T.; Wu, T.; Wu, Q.; Ye, C.; Hu, R.; Chen, W.; He, X. Real-time measurement of CO2 isotopologue ratios in exhaled breath by hollow waveguide based mid-infrared gas sensor. *Opt. Express* **2020**, *28*, 10970-10980.
(24)Westberg, J.; Wang, J.; Axner, O. Fast and non-approximate methodology for calculation of wavelength-modulated Voigt lineshape functions suitable for real-time curve fitting. *J. Quant. Spectrosc. Ra*. **2012**, *113*, 2049-2057.
(25)Axner, O; Kluczynski, P; Lindberg, A. M. A general non-complex analytical expression for the nth Fourier component of a wave-length-modulated Lorentzian lineshape function. *J. Quant. Spectrosc. Ra*. **2001**, *68*, 299-317.
(26)Weidmann, D; Wysock, G; Oppenheimer, C; Tittel, F. K. Development of a compact quantum cascade laser spectrometer for field measurements of CO2 isotopes. *Appl. Phys. B* **2005**, *80*, 255-260.
(27) Gordon, I. E.; Rothman, L. S.; Hill, C.; Kochanov, R. V.; Tan, Y.; Bernath, P. F.; Birk, M.; Boudon, V.; Campargue, A.; Chance, K. V.; Drouin, B. J.; Flaud, J. -M.; Gamache, R. R.; Hodges, J. T.; Jacquemart, D.; Perevalov, V. I.; Perrin, A.; Shine, K. P.; Smith, M. -A. H.; Tennyson, J. Toon, G. C.; Tran, H.; Tyuterev, V. G.; Barbe, A.; Császár, A. G.; Devi, V. M.; Furtenbacher, T.; Harrison, J. J.; Hartmann, J. -M.; Jolly, A.; Johnson, T. J.; Karman, T.; Kleiner, I.; Kyuberis, A. A.; Loos, J.; Lyulin, O. M.; Massie, S. T.; Mikhailenko, S. N.; Moazzen-Ahmadi, N.; Müller, H. S. P.; Naumenko, O. V.; Nikitin, A. V.; Polyansky, O. L.; Rey, M.; Rotger, M.; Sharpe, S. W.; Sung, K.; Starikova, E.; Tashkun, S. A.; Auwera, J. Vander; Wagner, G.; Wilzewski, J.; Wcisło, P.; Yu, S.; Zak, E. J. The HITRAN2016 molecular spectroscopic database. *J. Quant. Spectrosc. Radiat. Transfer* **2017**, *203*, 3–69.
(28)Werle, P. O.; Mücke, R.; Slemr, F. The limits of signal averaging in atmospheric trace-gas monitoring by tunable diode-laser absorption spectroscopy (TDLAS). *Appl. Phys. B* **1993**, *57*, 131-139.

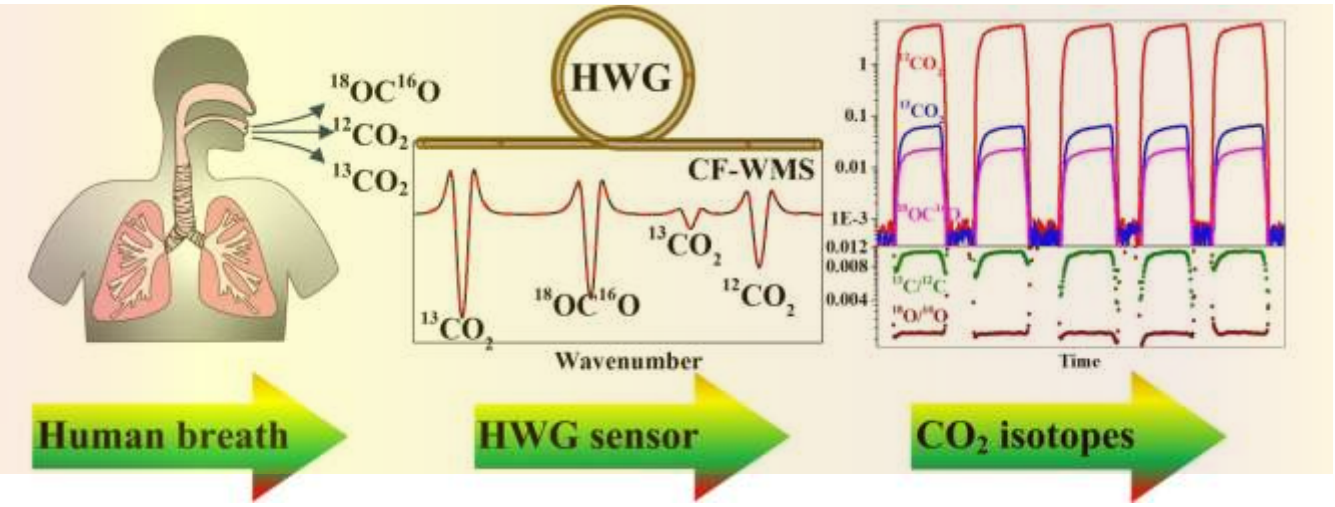

For Table of Contents Only